Blending Ferulic Acid Derivatives and Polylactic Acid into Biobased and Transparent Elastomeric Materials with Shape Memory Properties

Antoine Gallos, Jean-Marc Crowet, Laurent Michely, Vikram Raghuwanshi, Matthieu Mention, Valérie Langlois, Manuel Dauchez, Gil Garnier, Florent Allais

Blending ferulic acid derivatives and polylactic acid into bio-based and transparent elastomeric materials with shape memory properties

Antoine Gallos[1,], Jean-Marc Crowet[2], Laurent Michely[3], Vikram Raghuwanshi[4], Matthieu Mention[1], Valérie Langlois[3], Manuel Dauchez[2], Gil Garnier[1,4] and Florent Allais[1,4*]*

[1] URD Agro-Biotechnologies Industrielles (ABI), CEBB, AgroParisTech, 51100, Pomacle, France

[2] CNRS UMR 7369 MEDyC, Chaire MAgICS, Université de Reims Champagne-Ardenne, 51687 Reims Cedex 2, France

[3] Systèmes Polymères Complexes, Université Paris Est Créteil (UPEC), 2-8 rue Henri Dunant, 94320 Thiais, France

[4] BioPRIA, Department of Chemical Engineering, Monash University, Clayton, Australia

ABSTRACT: Thanks to its remarkable properties such as sustainability, compostability, biocompatibility and transparency, poly-L,L-lactide (PLA) would be a suitable replacement for oil-based polymers should it not suffer from low flexibility and poor toughness, restricting its use to rigid plastic by excluding elastomeric applications. Indeed, there are few fully bio-based and biodegradable transparent elastomers -PLA-based or not- currently available. During the last decades, many strategies have been investigated to soften PLA and enhance its toughness and elongation at break by using plasticizers, oligomers or polymers. This work shows how a ferulic acid-derived bio-based additive (BDF) blends with a common rigid and brittle commercial grade of polylactic acid to provide a transparent non-covalently crosslinked elastomeric material with shape-memory behavior exhibiting an elongation at break of 434% (vs. 5.6 for pristine PLA). Through a Structure-Activity Relationship analysis conducted with BDF analogues, and a modelling study, we propose a mechanism based on π-π stacking to account for the elastomeric properties. Blending ferulic acid derivatives to polylactic acid generates a new family of fully sustainable transparent elastomeric materials with functional properties such as shape memory.

KEYWORDS: Polylactic acid; sustainable elastomer; shape memory; mechanical properties; material science

1. Introduction

PLA is a thermoplastic polyester made of lactic acid. It is fully sustainable,[1] compostable and biodegradable under specific conditions,[2] recyclable,[3] transparent,[4] and biocompatible.[5] PLA

forms a family of polymers due to the asymmetric carbon on its backbone. Indeed, the two enantiomers (L-Lactic acid and D-Lactic acid) lead to a variety of polymers with properties correlated to the ratio and distribution of L and D units.[6,7] This study focuses on one of the most common commercial grades of PLA containing 95.7 % of L-lactic acid units. Despite their high modulus and attractive transparency, industrial grades of PLA are limited in use by their low elongation at break (<10%) and their lack of flexibility.[8] Many studies have investigated conventional (e.g., polyethylene glycol) or bio-based plasticizers (e.g., lactic acid oligomers, glycerol, citrate esters) to improve both PLA elongation at break and flexibility.[9–12] Nevertheless, plasticizing PLA remains challenging because of phase separation and leaching phenomena.[13] These two issues often lead to a diminution in plasticization over time which decreases the mechanical properties of PLA blends as aging progresses over weeks or months. For instance, mixing PLA with thermoplastic polyurethanes (TPU) or polyamide (PA) has led to shape-memory blends exhibiting excellent mechanical properties (storage modulus > 2 GPa and elongation at break higher than 200% for PLA/PA blends) as well as high shape memory index (>80% for PLA/TPU blends).[14,15] Mixing PLA with polycaprolactone (PCL) can also increase mechanical properties by softening PLA.[16] However, even if it does not necessarily impedes thermo-mechanical properties, the immiscibility between PLA and TPU, PA or PCL, led to phase separation responsible for the whitish and opaque appearance of the materials. Moreover, TPU has poor recyclability and biodegradability even in controlled compost conditions.[17] In a more common way, elastomers and thermoplastics elastomers lack of sustainable alternatives leading to the generation of a large amount of plastics waste.[17–20]

Herein, we transform a common commercial grade of brittle PLA into a transparent and highly flexible blend with elastomeric behavior at room temperature using a bio-based additive. PLA

was blended at different ratios ranging from 10 wt% to 40 wt% with Bis-O-feruloyl-1,4-butanediol (BDF). BDF is a bio-based additive synthesized from lignocellulose-derived ferulic acid and cellulose-derived 1,4-butanediol (Figure S1, Table S1) that does not exhibit any endocrine activity on estrogen receptors.[21–23] In this work, one must note that PLA was simply blended at 180 °C for 15 minutes with BDF without the need of chemical reagent or crosslinking agent. Developing a new class of fully biobased elastomeric blends without any covalent cross-linking is of great interest especially since we only used hydrolysable ester moieties. This make the material suitable to biological and chemical recycling.[3] Such an elastomeric blend would be a sustainable alternative to oil-based elastomer and/or non-recyclable/non-biodegradable elastomeric blends such as PLA/TPU. Moreover, the transparency of the material would be interesting in combination with other properties (e.g., elastomeric behavior, UV-absorbance, good processability) for many applications including UV-shielding.[24] Indeed, not only a colorless and reprocessable material is more convenient to customize with pigments than an opaque/colored or non-reprocessable material, but it also opens a wide range of uses where transparency is not required (e.g., textile, flooring, goods).

This study also aims to understand the structural mechanism responsible for the elastomeric behavior. This comprehensive work would help to reproduce this result with other biopolymers to extend the field of sustainable alternatives for elastomeric materials. The thermo-mechanical properties of the blends were first studied. A sudden and unexpected change of behavior from thermoplastic to elastomeric appears as the BDF ratio increases from 20 wt% to 25 wt%. Two approaches were investigated to elucidate this phenomenon. First, a Structure-Activity Relationship (SAR) study with the synthesis of specific structural BDF analogs evidencing the role of each chemical moiety; second, molecular modelling to explore the spatial molecular

configuration of BDF in the PLA chains and quantify interactions and energy minima. Last, a mechanism based on π-π stacking is proposed to account for the determined SARs.

2. Experimental Section/Method

Material

PLA IngeoTM Biopolymer 4043D from NatureWorks was used in this study. It contains 95.7% of L-lactic acid units according to the certificate of analysis from the manufacturer. M_n is 106×10^3 g.mol^{-1} and M_w is 168×10^3 g.mol^{-1} according to literature.[25] The dispersity (Đ) is approximately 1.6. The glass transition temperature (T_g) is between 55 and 60 °C and the elongation at break is 6%. *trans*-Ferulic acid (≥99%) and benzoyl chloride (99%) were supplied by Sigma-Aldrich. Octanoic acid (98%) and 1,4-butanediol (99%) were purchased from Alfa-Aesar.

Methods

^{1}H NMR spectra were achieved on a Brucker Fourier 300 (300 MHz) and calibrated with Acetone-d_6, protons signals at δ 2.05 ppm. Data are reported as follows: chemical shift (δ ppm), integration, multiplicity (s = singlet, d = doublet, dd = doublet of doublets), coupling constant (Hz) and assignment. ^{13}C NMR spectra were recorded on a Brucker Fourier 300 (75 MHz) and were calibrated with Acetone-d_6, signals at δ = 206.26 and 29.84 ppm. Data are reported as follows: chemical shift (δ ppm) and attribution. NMR spectra assignments were achieved using COSY, HMBC and HSQC spectrum. High resolution mass spectrometry was performed on an Agilent 1290 system, equipped with a 6545 Q-TOF mass spectrometer (Wilmington, DE, USA) and a PDA UV detector. The source was equipped with a JetStream ESI probe operating at

atmospheric pressure. Melting points were recorded on a Metler Toledo MP50 Melting Points system, T initial = 40 °C, heating 3 °C per minute until 200 °C with ME-18552 sample tubes.

Synthesis of biosourced additives

Biocatalytic syntheses and characterizations of Bis-*O*-dihydroferuloyl-1,4-butanediol (BDF) and Butane-1,4-diyl-bis(3-(3,4-dimethoxyphenyl)propanoate) (BDFMe) were synthesized as reported elsewhere.[26] Ferulic acid was esterified in ethanol and hydrogenated into ethyl-dihydroferulic acid prior the transesterification with butanediol in presence of *Candida antartica* lipase B (CAL-B) at 80°C for 4 hours under vacuum. BDF was then purified from the bulk by recrystallization in ethanol after the filtration of CAL-B beads. BDFMe was obtained through the methylation of the phenolic functions of BDF with methyl iodide and potassium carbonate in anhydrous DMF.

Synthesis of Bis-O-benzoyl-1,4-butanediol (BDB):

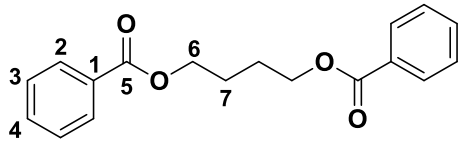

1,4-Butanediol (C = 0.6 M) and triethylamine (2.2 equiv) were stirred in anhydrous CH_2Cl_2 at 0 °C under N_2. Benzoyl chloride (2.2 equiv) was slowly added and the mixture was stirred 5 min at 0 °C before warming up at room temperature. The flow of N_2 was stopped and the reaction was stirred for 6 h. The mixture was diluted in CH_2Cl_2 and H_2O, the organic layer was washed with saturated $NaHCO_3$, dried over anhydrous $MgSO_4$, filtered and concentrated under reduced pressure to afford a white powder (97% yield, mp 72.2 °C).

UV-vis: λ_{max} (EtOH, nm) 202, 229, 273. IR: ν (cm^{-1}) 1703 (C=O), 1580 (C=C aromatic), 1268 (C-O). NMR ^1H δ_H (300 MHz, Acetone-d_6): 1.98 (m, 4H, H7), 4.41 (m, 4H, H6), 7.51 (m, 4H,

H3), 7.63 (m, 2H, H4), 8.03 (m, 4H, H2) ppm. ^{13}C δ_C (75 MHz, Acetone-d_6): 26.3 (C7), 65.2 (C6), 129.4 (C3), 130.2 (C4), 131.4 (C1), 133.9 (C2), 166.7 (C5) ppm. HRMS *m/z* $[M+H]^+$: Exact mass: 299.1283; found: 299.1289

Synthesis of Bis-O-octanoyl-1,4-butanediol (BDOct):

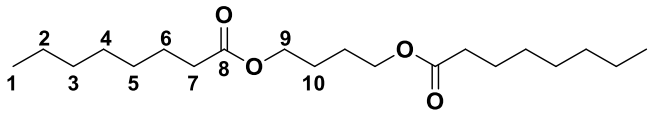

1,4-Butanediol and octanoic acid (4 equiv) were stirred at 60 °C with CAL-B (10 % w/w) under reduced pressure (1 mbar) for 3 days. After cooling at room temperature, the mixture was dissolved in CH_2Cl_2 and filtered to remove the CAL-B beads. CH_2Cl_2 was removed under vacuum, the crude oil was diluted in ethyl acetate and washed with saturated $NaHCO_3$. The organic layer was dried over anhydrous $MgSO_4$, filtered and concentrated under reduced pressure to afford a light-yellow oil (98% yield, mp 10.1 °C).

UV-vis: λ_{max} (EtOH, nm) no absorbance. IR: ν (cm^{-1}) 2924 (C-H), 1734 (C=O), 1160 (C-O). NMR ^1H δ_H (300 MHz, DMSO-d_6): 0.85 (t, 6H, J = 7.3 Hz, H1), 1.24 (m, 16H, H2,3,4,5), 1.51 (m, 4H, H6), 1.60 (m, 4H, H10), 2.27 (t, 4H, J = 7.3 Hz, H7), 4.02 (m, 4H, H9) ppm. ^{13}C δ_C (75 MHz, DMSO-d_6): 13.9 (C1), 22.0 (C2), 24.5 (C6), 24.8 (C10), 28.3 (C3), 28.4 (C4), 31.1 (C5), 33.5 (C7), 63.2 (C9), 173.0 (C8) ppm. HRMS *m/z* $[M+H]^+$: Exact mass: 343.2848; found: 343.2845

Hot-melt processing

The blends were prepared by hot-melt processing using an internal mixer Haake Rheomix from ThermoFisher Scientific. The speed of the rotors was set at 50 rpm and the temperature was fixed at 180 °C. The pure PLA was first incorporated and solely mixed during 2 minutes, then

the biosourced additives were added and blended during 13 minutes. The name of the compounds and their composition are given in Table S1.

Tensile test & shape-memory experiments

The blends were injected into two sets of tensile test specimen. The first set of dogbones was injected according to ISO 527-2-5 A (dimensions: 74.0 × 4.1 × 2.0 mm^3) using a bench-scale injection system from DSM (Xplore microinjection mold IM 12). The melting temperature was set at 160 °C and the mold was kept at room temperature. The injection pressure was set at 1.6 × 103 $kN.m^{-2}$. The second set of specimens was prepared by hot-melt pressing using a heat press set at 160 °C. The pressure of the plates was set at 5 × 10^3 $kN.m^{-2}$ during 5 minutes. The mold was then cooled at room temperature using a chiller prior removing the non-standardized dogbones (dimensions: 50.0 × 4.0 × 1.0 mm^3). Thin films (dimensions: 90.0 × 90.0 × 0.2 mm^3) were prepared using the heat press following the experimental conditions of non-standardized dogbones.

The dogbones samples were measured using the Instron tensile tester (model 5965) equipped with specimen holder Instron-2701-221 and the processing software Bluehill Universal V4.03 (Illinois Tool Work Inc). The displacement rate was 10 $mm.min^{-1}$ and the room temperature was 23 °C. Each test was performed at least in triplicate.

The cycles (**Figure 1c**) were conducted following an extension of the dogbones until 30 mm (corresponding to an elongation of 150% and an extension time of 180 s). The dogbones were hold for 120 s (the force versus time was still recorded). The dogbones were then unclamped and led to relax 2 h at 23 °C and 50% relative humidity between each cycle (Figure S2).

Transparency

The transparency of the blends was characterized using a Cary 60 UV-Visible spectrophotometer from Agilent. The crude PLA was used as a reference and the blends of PLA containing various content of BDF were normalized according to the pure PLA to provide a direct comparison. As reported in Figure S3, the whole material exhibits the same absorbance in visible wavelengths (from 400 nm to 800 nm), meaning the addition of BDF fully preserves the transparency of pure PLA. All blends containing BDF shows a higher absorbance in UV wavelengths (from 250 nm to 350 nm) that is due to the phenolic moieties of BDF.

Differential Scanning Calorimetry (DSC)

Differential Scanning Calorimetry (DSC) experiments were performed on the PLA blends using a TA Q20 from TA Instruments. The cooling and heating ramp from -80 °C to 200 °C were performed at 10 °C.min-1 under nitrogen atmosphere. Two heating and cooling cycles were performed for each sample without any thermal treatment. The data recorded for the first heating, corresponding to the thermal history, are given in Figure S4a and Table S2. The results for the second heating are given in Figure 2a and Figure 2b, and the corresponding T_g values are provided in Table S2. A heating ramp was done for each sample after thermal treatment at 80 °C for 48 hours. These data, corresponding to thermal history after annealing, are given in Figure S4b and Table S2. The percent crystallinity of PLA and BDF in blends was calculated with respect to the weight fraction of each component and using the difference between melting enthalpy and cold crystallization enthalpy.[27] The value used for the 100 % crystalline PLA was 93 $J.g^{-1}$ and that for 100% crystalline BDF was 115 $J.g^{-1}$. The crystallinity of the blends evolves

slowly as they mainly remain amorphous at room temperature after the process because the crystallized content of PLA (χc_PLA) is close to 0% (Figure S4 and Table S2).

Size Exclusion Chromatography

Blends of PLA containing BDF were easily dissolved in THF as well as pure PLA to measure the molar masses by Size Exclusion Chromatography (SEC). The experiments were performed using a PL gel Mixed-D column with a Differential Refractometer 1260 Infinity from Agilent and with polystyrene (PS) standards (Varian Standards). THF was also used as eluent at 1.0 $mL.min^{-1}$. The following Mark-Houwink coefficient were used ($K = 0.406$ and $\alpha = 1.0486$).[28] Results are given in Table S3.

NB: Such materials are also fully soluble in $CHCl_3$ which is a good solvent for PLA.

Dynamic Mechanical Analysis

The Dynamic Mechanical Analysis (DMA) was performed with a DMA Q800 from TA Instrument, under traction solicitation at a frequency of 1 Hz, over a temperature range of -140 to 140 °C at a heating rate of 3 $°C.min^{-1}$.

The DMA of the blends indicates a competition between an increase of the storage modulus (E') due to a change of the crystallinity initiated by BDF and a decrease of the E' due to the plasticizing effect of BDF (Figure 2c). The loss factor (Tan δ) (Figure 2d) shows a phase separation with two peaks for PLA-BDF40. The first one can be attributed to a semi-crystalline phase mainly composed of α or δ phase that can be found in PLA-BDF10. The second can be attributed to a highly plasticized amorphous phase.

X-Ray Diffraction

X-Ray Diffraction (XRD) experiments were performed on pure BDF and pure PLA as well as on blends of PLA containing from 10 wt% to 40 wt% of BDF (Figures S5 and S6). Samples were characterized without any thermal treatment and after a thermal treatment of 80 °C for 48 hours.

The structures were analyzed using a D8 Advance Bruker diffractometer with Cu Kα radiation (λ = 0.1542 nm), between 5 and 55° with a step of 0.02°.

Non-annealed samples indicate the very crystalline structure of BDF after synthesis, with multiple and well-defined peaks at 11.1°, 14.8°, 16.9°, 19.5°, 22.0°, 22.5°, 23.2°, 25.5° and 27.1° as shown on Figure S5. Non-annealed PLA reveals a classical semi-crystalline structure with a single visible peak at 16.9°.[29] Non-annealed blends of PLA containing various content of BDF have the same semi-crystalline structure than pure PLA, with the single peak around 16.9°. This is in full accordance with the DSC experiments (Figure S4a).

The crystalline structure of BDF did not change after annealing at 80 °C for 48 hours, as shown on Figure S6. Pure PLA crystallized after such thermal treatment and exhibited a large peak at 16.9° and two very small peaks at 19.0° and 22.5°. This is in accordance with the δ crystalline phase of PLA.[30,31] Blends of PLA containing 30 wt% and 40 wt% of BDF show a crystalline structure with the superposition of the crystalline signatures of both PLA and BDF, which is in full accordance with the results of the DSC experiments (Figure S4b). The crystalline structure of PLA appears with a slight shift (main peak located at 17.1°). A shift was already reported to describe the transition from an δ to an α phase.[29,30] Such shift also occurred without annealing treatment, but is less visible due to the low degree of crystallinity. The formation of an α crystalline phase in blends of PLA is in accordance with the DMA results (Figure 2c). The

results of PLA containing 10 wt% and 20 wt% are more difficult to interpret because the specific peaks of BDF located at 11.1°, 25.5° and 27.1° are not clearly visible on Figure S6. Moreover, as the peaks of crystalline PLA located at 19.0° and 22.5° are very close to that of BDF, it is difficult to assign the crystalline signature to a superposition of crystalline PLA (α phase) and crystalline BDF, or to assign it to the sole signature of crystalline PLA (α phase). The DSC experiments (Figure S4b) only revealed a crystalline structure corresponding to PLA at 10 wt% and 20 wt% of BDF.

Molecular Dynamic Simulations

BDF molecules were studied by molecular dynamics (MD) in a matrix of polylactide (PLA; 3 chains of 500 lactic acid units). All simulations were performed with the GAFF force field.[32] The BDF topology was generated with Antechamber and the PLA topology proposed by Glova et al. in 2018 was used.[33,34] The PLA system simulated by McAliley et al. was selected as starting structure.[35] 60 or 105 BDF were placed in the PLA box on a grid every 1.36 and 1.09 nm to generate a concentration of 20 wt% and 30 wt% of BDF. The coordinates are reduced ten times in the XYZ dimensions to prevent steric clashes due to the insertion and expansion to their original size during the minimization step. Simulations with 1 BDF in the PLA matrix and simulations of a box with only BDF molecules (100 BDF) were also carried on. Three repetitions were made for each system. All the systems studied were minimized by a steepest descent of 1,000 steps before NVT simulation of 100 ps. NPT production simulations were run for 100 ns with a 2 fs time step. Temperature was coupled at 550 K for PLA and 400 K for BDF systems and pressure was coupled at 1 bar using the weak coupling Berendsen algorithm.[36] τT and τP were set at 1 ps and 1 ps, respectively with a compressibility of 4.5 × 105 (1/bar). 550 K and 400

K are above the fusion temperature of PLA and BDF. Pressure was coupled isotropically and periodic boundary conditions (PBC) were used. Electrostatic interactions were treated by using the particle mesh Ewald (PME) method with a short-range cut-off of 1 nm.[37] The van der Waals interactions were truncated at 1 nm. Trajectories were performed and analyzed with GROMACS 2018.4 tools.[38] Trajectories and structures were also analyzed with MDAnalysis and VMD softwares.[39,40] To compute contacts between molecules, a cut-off of 3 Å was selected and π-π interactions was computed as described in Fu et al.[41] The distance between the aromatics center of mass must be lower than 7.5 Å. For parallel configurations, the angle between aromatic planes has to be lower than 40°. For perpendicular configurations, the angle between aromatic plans has to be greater than 50° and one of the aromatic ring has to be above the plane of the other one within an angle lower than 40° according to the normal of the first aromatic plane (Figure S9). Simulations were performed above the melting temperature to accelerate the equilibration and study properties of the mixtures in a melt. Experimentally, to blend BDF and PLA materials, these compounds are brought to high temperature and interactions arising at this temperature should be representative of the initial state of the blends and should also be conserved during cooling.

3. Results and discussion

3.1. Mechanical and optical properties

The stress-strain curves of PLA-BDF blends are presented as a function of BDF content in **Figure 1a**. Materials are noted "PLA-BDFX" where "X" corresponds to the content of BDF (from 10 wt% to 40 wt%). Two distinct regimes are observed. In the first, corresponding to BDF

of 0 wt% to 20 wt%, the PLA-BDF materials are plastic, showing a progressive plasticization with decreasing Young's modulus (from 1 GPa to 0.6 GPa) and increasing elongation at break (from 4% to 10%, where some cracks started to appear) as increases the BDF content. In the second regime, corresponding to BDF content of 25 wt% to 40 wt%, the PLA-BDF materials are elastomeric, showing significant increase in elongation at break, reaching above 400%. This transition plastic to elastomeric is sudden and occurs at a BDF content between 20 wt% and 25 wt%. This increase is well beyond the level expected from a pure plasticization mechanism that simply relies on an increase in mobility of the polymer chains.[42,43] These results indicate a transition from plastic to elastomeric behavior after a critical BDF content of 25 wt%. This observation is quite surprising since the incorporation of plasticizers generally leads to a phase separation and a loss of cohesion in the blends involving degradation of the mechanical properties.[13,44,45] Indeed, strong molecular material cohesion is required to sustain such a significant elongation at break as that measured. This cohesion can be seen on the dogbones during the tensile experiments, where the whole sample deforms (**Figure 1b, Caption for movie S1, Caption for movie S2**). Shape memory behavior demonstrating the reversible elasticity of the blends was quantified through tensile tests and relaxation cycles performed on PLA-BDF30 (Figure1c). Full recovery was achieved after four cycles of elongation at 150% and relaxation. Deformation and recovery experiments were also conducted on a PLA-BDF30 thin film to qualitatively highlight the shape memory behavior after multi-axial deformations (**Figure 1d**).

The transparency of the blends was also quantified by UV-Visible spectroscopy (**Figure S3**). In the visible wavelengths range, the addition of BDF up to 40 wt% does not decrease the transparency of the PLA blends remaining as transparent as the original PLA material. This is in accordance with both a high affinity between BDF and PLA, and a good dispersion of the bio-

based additive in the blend. Transparency in the visible wavelengths is consistent with very miscible blends or with the formation of nanoscale domains. Moreover, blending BDF extends the absorbance from 200 nm to 350 nm, as PLA only absorbs from 200 nm to 240 nm, thus providing significant anti-UV properties.[4] This increase in absorption range in the UV wavelengths is due to the aromatic moieties of BDF.[46]

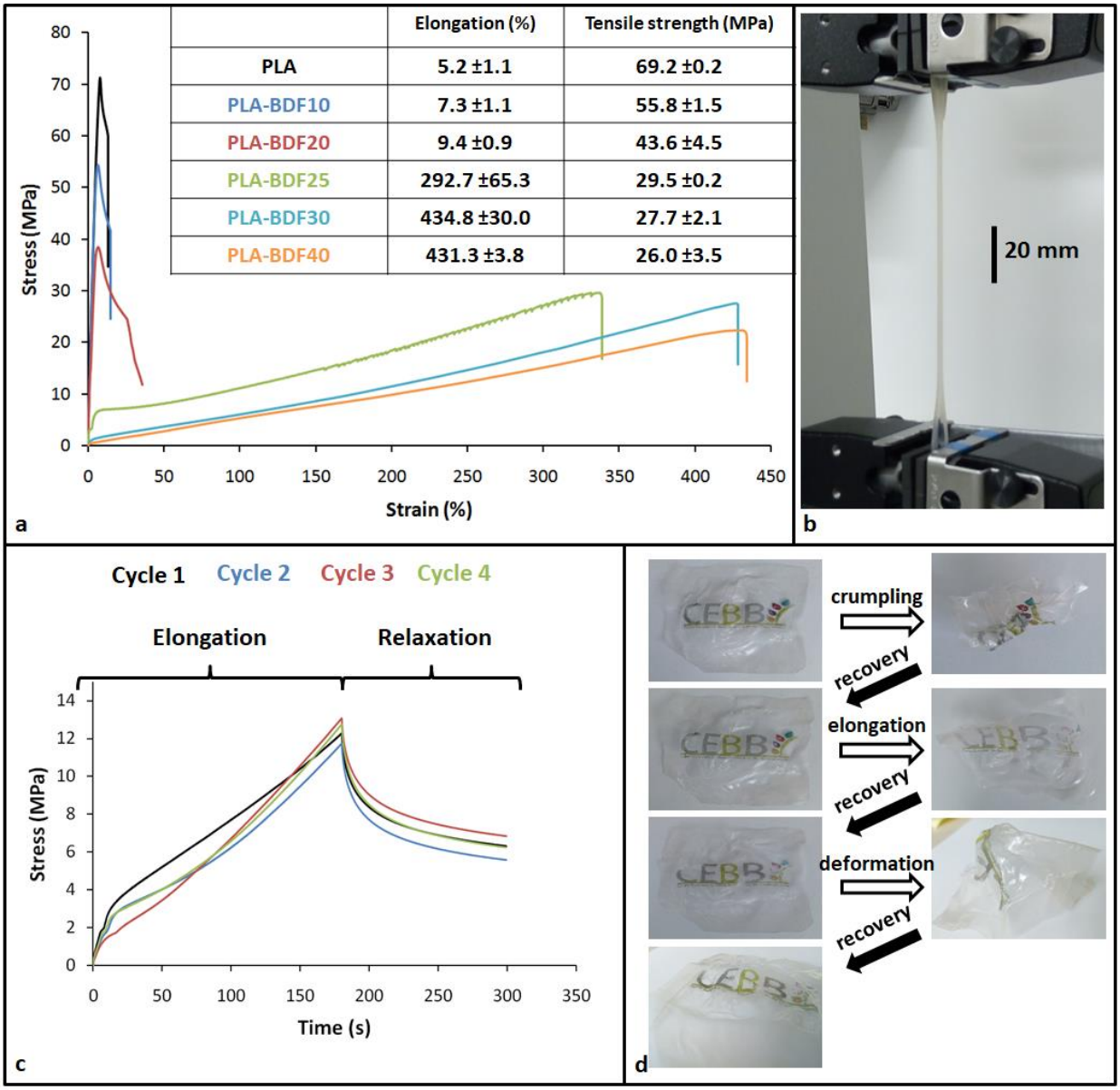

Figure 1: Mechanical properties and shape-memory behavior of PLA-BDF blends.

a. Tensile test experiments. PLA containing up to 20 wt% of BDF shows a plastic behavior (high modulus and low irreversible deformation). PLA containing more than 25 wt% of BDF exhibits an elastomeric behavior (low modulus and high reversible deformation).

b. Specimen of PLA-BDF30 under tensile testing at 400% deformation. The whole specimen deforms- not only the middle part. This indicates the strong cohesion of the material.

c. Elongation and relaxation cycles by tensile testing on PLA-BDF30. The stress was measured during the elongation to 150% followed by 2 minutes of relaxation. The sample fully recovered its original shape after 2 hours unclamped at room temperature prior to another cycle. The reproducible values of the 4 consecutive cycles are consistent with shape memory behavior.

d. Multiple hand deformations and self-recovery at room temperature within minutes on a 200 µm thick film of PLA-BDF30.

3.2. Characterization of amorphous and crystalline phases

The thermal properties of the blends were investigated by Differential Scanning Calorimetry (DSC) (**Figure 2a**). A classical semi-crystalline behavior of the blends was observed. A single T_g is reported (Figure 2a); this generally indicates full miscibility of the two components of the blends in the amorphous phase. The Fox's equation was drawn using the T_g of crude PLA (56.4 °C) and that measured for pure BDF (-19.1 °C). The T_g evolution of the PLA blends as a function of BDF content (**Figure 2b**) exhibits a deviation from the Fox's equation represented by the dotted curve, showing that the miscibility is good but not perfect.[44] Crosslinking with covalent bonding between PLA and BDF would be consistent with such cohesive material with a non-perfect miscibility. However, covalent crosslinking between PLA and BDF is not consistent

with the semi-crystalline behavior measured for the blend. A thermal annealing above T_g (80 °C for 48 hours) was performed to force crystallization of the amorphous phase of the blend. The crystalline phases were characterized by DSC and X-Ray Diffraction (XRD). The thermal history recorded on **Figure S4b** exhibits a high crystallinity. A single melting enthalpy corresponding to an α crystalline phase is present for all materials. A second melting enthalpy, consistent with a melting enthalpy corresponding to crystalline BDF, can be seen for the materials with a content of BDF higher or equal to 25 wt%. This thermal treatment revealed BDF to remain amorphous at 10 wt% and 20 wt%, whereas it crystallizes at 25 wt%, 30 wt% and 40 wt% (**Figure S4b and Table S2**). The crystalline phases were characterized by XRD before and after thermal treatment (**Figures S5 and S6**) and were attributed to a simple superposition of an α phase (or δ phase) of PLA and crystalline BDF. As described in the experimental part, no new crystalline structure was evidenced, demonstrating that the blends contain amorphous PLA and BDF able to crystallize in separated phases, confirming the DSC results. The loss factor (Tan δ) was measured by Dynamic Mechanical Analysis (DMA) to corroborate the DSC and XRD analyses. The two peaks observed for PLA-BDF40 (**Figure 2d**) confirm that the BDF-PLA miscibility in amorphous phase is not perfect. The first peak corresponds to an amorphous blend mainly composed of PLA with a large amount of BDF acting as plasticizer (**Figure 2c**). The second peak is attributed to a semi-crystalline blend composed of PLA with a low amount of BDF acting as nucleating agent for the α or δ crystalline phases of PLA (**Figures S5 and S6**). The compatibility between PLA and BDF allows a continuous amorphous phase to be formed with one single T_g. When the weight content of BDF reaches 25 wt%, small clusters of BDF are formed within the PLA matrix without disrupting the continuity of the amorphous phase. These

clusters are big enough to crystallize at the proper temperature. The interface between PLA and BDF is small enough to allow transparency in the visible wavelengths (**Figure S3**).

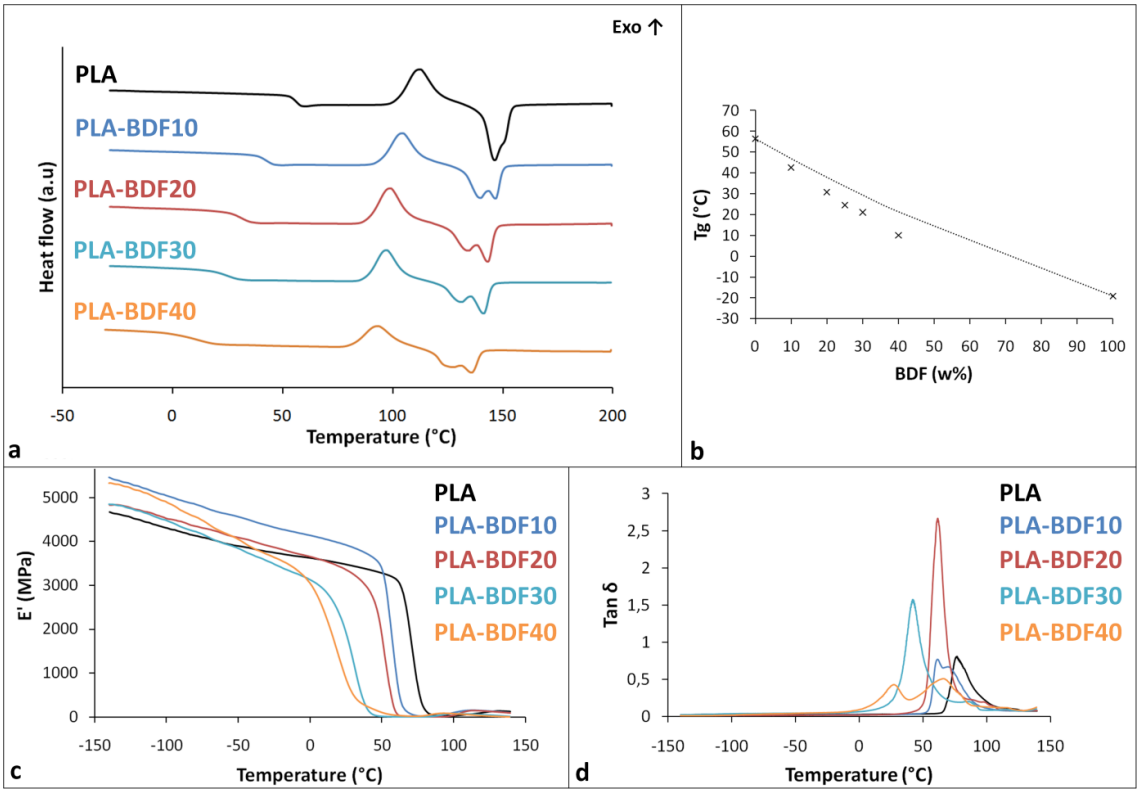

Figure 2: Differential Scanning Calorimetry and Dynamic Mechanical Analyses of PLA blended with different concentrations of BDF.

a. DSC experiments of PLA blends varying in BDF content (0 wt% to 40 wt%) after erasing thermal history. The semi-crystalline behavior of PLA is preserved. Only one T_g appears for each blend meaning there is one continuous amorphous phase made of miscible PLA and BDF.

b. Evolution of the glass transition temperature (T_g) as a function of BDF content in blends. The continuous curve was calculated from the Fox's equation (empirical). The evolution of the T_g blends below prediction indicates the miscibility of BDF in PLA is not perfect.

c. Storage modulus (E') of the blends. All the blends show an increase of modulus prior to T_g and a decrease of their respective T_g compared to PLA. This is consistent with a competition between two antagonistic effects. There is first an increase in crystallinity and crystalline transition from δ-form to α-form where BDF acts as a nucleating agent and increases E'. Second, the plasticization of the fully amorphous phase in blends decreases both E' and T_g.

d. Loss factor (Tan δ) of blends. PLA-BDF40 shows two peaks. The first one is attributed to an amorphous and highly plasticized PLA blend containing a large amount of BDF. The second indicates a semi-crystalline blend analog to the PLA-BDF10 with low BDF induced plasticization and an increase in the PLA crystallinity.

3.3. Structural mechanism

PLA containing more than 25 wt% BDF showed phase separation and the formation of small clusters of additive. The molecular cohesion of such blends is maintained by a combination of "PLA–PLA", "PLA–BDF" and "BDF–BDF" interactions which ensures the continuity of the amorphous phase, explaining the transition from a plastic to an elastomeric behavior. Shape-memory polymers usually have at least one covalently bonded network.[47] While natural rubber requires vulcanization to develop its elastomeric behavior, thermoplastic polyurethanes only have non-covalent interactions between the polymeric chains. Therefore, two mechanisms can be considered to describe these interactions: (1) the formation of a crosslinked network with chemical bonding, and (2) a network connected with physical bonding only.

Any covalent crosslinking between PLA and BDF has to be ruled out due to the semi-crystalline behavior of the blends. Moreover, the molar masses and the dispersity (Đ) of the PLA

measured in the blends by Size Exclusion Chromatography (SEC) support this claim. **Table S3** shows the results of the SEC experiments conducted on PLA and PLA blended with BDF. A slight decrease of average molar masses combined with a moderate increase of dispersity is consistent with processing with a high shear mixer that can break some polymeric chains.[25] The preservation of the molar masses and dispersity of PLA after blending demonstrates that no chemical reaction occurs (e.g., chain scission, transesterification, reticulation) between components during the hot-melt process. Moreover, the complete solubility of PLA blended with BDF in THF further confirms the absence of any covalent crosslinking. Crosslinked network polymers, such as cured thermoset or vulcanized rubber, are insoluble. Thereby, a network connected by physical bonding appears as the PLA-BDF structural model most consistent with the results from the crystallinity, solubility and chemical analyses of the blends.

3.4. Structure-Activity Relationship by molecular design

A Structure-Activity Relationship (SAR) study was initiated to correlate the chemical structure of the additives with the thermo-mechanical properties of the blends. A series of BDF analogs was synthesized and blended in PLA at a content of 30 wt%. This was to quantify the impact played by each chemical moiety on blend miscibility and to identify the chemical parameters required to achieve a cohesive structure (**Figure 3a**). Three key structural features of BDF were studied: 1) the hydroxyl group of phenolic moieties, 2) the aliphatic chain between the ester moieties, and 3) the aromatic ring. Tensile testing and DSC experiments were performed to determine the effectiveness of this new series of additives using PLA-BDF30 as a reference. PLA-BDFMe30 - that is a BDF with its phenol methylated - has an elastomeric behavior analog to PLA-BDF30 (**Figure 3b**) and a single T_g (**Figure 3c**). Similarly, PLA-BDB30 – a BDF

analogue with no phenol and the aromatic rings directly connected to the ester moieties - is also elastomeric (Figure 3b) and has a single T_g (Figure 3c). These new results demonstrate that: (1) replacing free phenol moieties with methoxy moieties on the aromatic ring, and (2) removing the aliphatic chain between the aromatic ring and the ester do not prevent the elastomeric properties of PLA blend, but provide valuable tools to tailor them (e.g., by modifying hydrogen bonding extent, steric hindrance and free volume, T_g or crystallinity). Finally, PLA-BDOct30 – a BDF analogue where the aromatic rings are replaced by aliphatic chains - exhibits a plastic behavior (Figure 3b) and has a clear phase separation with a melting enthalpy of BDOct at 14 °C (Figure 3c), indicating that aromatic moieties are required to ensure elastomeric behavior and cohesion of the blend. This SAR study undoubtedly demonstrates that both a functional design of hydrophilic (esters), hydrophobic (–CH_2–, –CH_3) and aromatic moieties (benzene rings), combined to a sufficient flexibility of the additive, contribute to the cohesion of the blend. Literature reports π-π stacking as a keystone to shape-memory properties observed in various polymeric materials.[48,49] Assuming that such a π-π stacking occurs between the aromatic rings of the BDF molecules would be consistent with the hypothesis of a physical bonded network explaining the elastomeric behavior of our blends after the phase separation occurring at 25 wt% BDF.

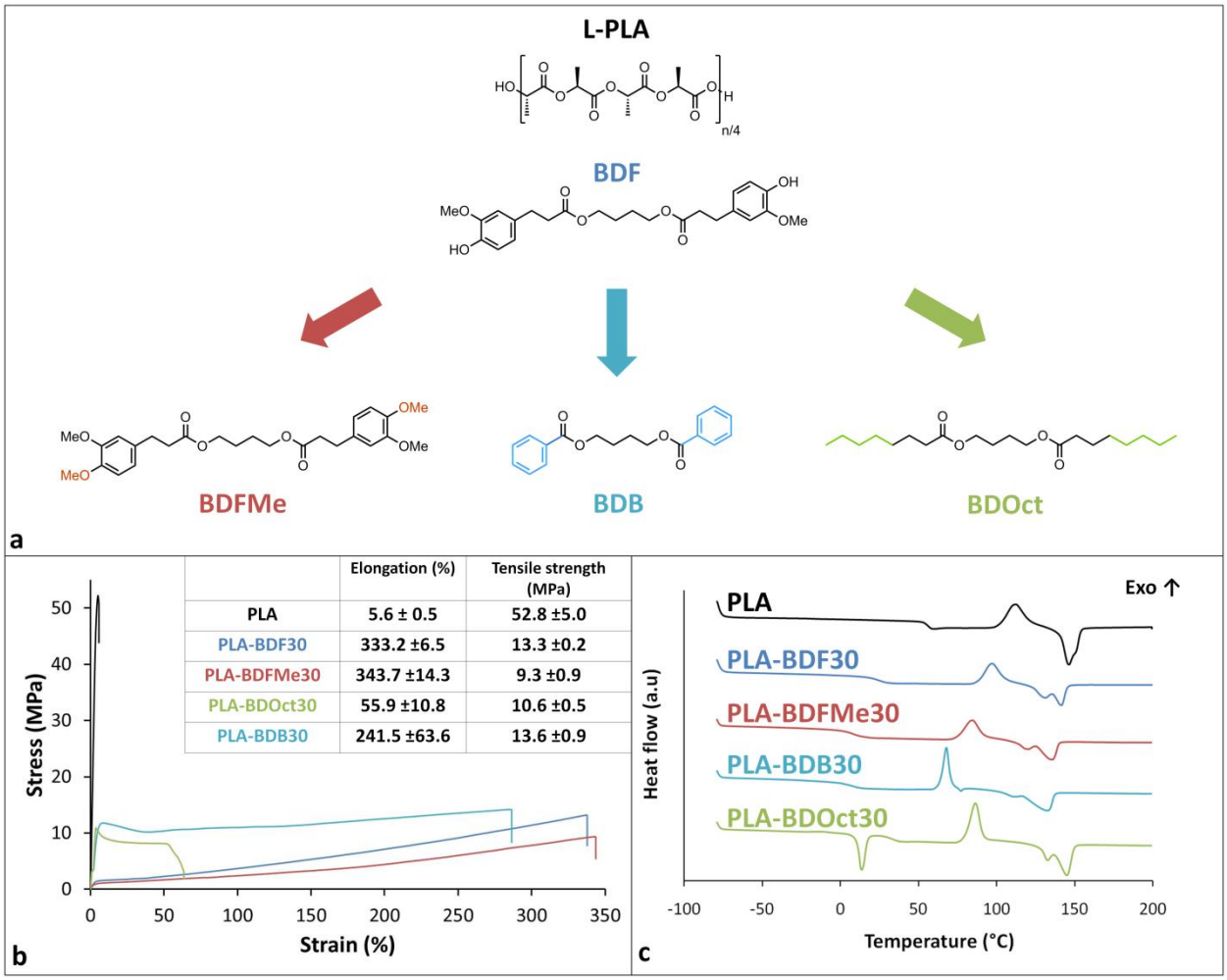

Figure 3: Modulating key chemical features and characterizing their effects on the blends

a. Synthesized additives were blended in PLA to elucidate the mechanism of miscibility and the role of chemical functionalities in the cohesiveness of the blends. BDFMe tests the role of phenolic moieties. BDB explores the influence of polar and apolar moieties close to the aromatic rings. The effect of removing the aromatic rings was analyzed with BDOct.

b. Tensile testing of blends. PLA-BDFMe30 shows an elastomeric behavior; the phenolic moieties are not important. PLA-BDB30 displays an elastomeric behavior; molecular flexibility and hydrophilic/hydrophobic layout are important but not key parameters. PLA-BDOct30 has a plastic deformation; aromatic rings are imperative for elasticity.

c. DSC experiments conducted on blends after erasing their thermal history. Thermal behaviors of PLA-BDFMe30 and PLA-BDB30 are analog to PLA-BDF30. PLA-BDOct shows important phase separation; removing the aromatic rings led to phase separation.

3.5. Modelling to quantify molecular interactions

A modelling approach was conducted to investigate the potential interactions arising between BDF molecules and PLA. Molecular dynamic simulations of PLA-BDF20 and PLA-BDF30 blends were generated (**Figure 4a**). Calculations show that BDF can adopt many conformations in PLA-BDF20 where several molecules are isolated while others form small and loose clusters. Those clusters appear much larger in PLA-BDF30 and almost no single molecule of BDF is observable. Contacts arising between BDF and PLA were also computed (**Figure 4b and Figure S11**). The number of contacts between BDF molecules increases while contacts between BDF and PLA decrease as the content of BDF increases from 20 to 30 wt%. In PLA-BDF20, every BDF molecule interacts with PLA which is consistent with the good miscibility of BDF in PLA measured at this content. In PLA-BDF30, several BDF molecules have no interactions with PLA, corresponding to the formation of clusters containing only BDF and to the phase separation. The distribution of the distance between the center of mass of the two aromatic rings of each BDF in PLA-BDF30 was computed (**Figure 4c**). The aromatic rings of BDF can evolve between close and distant position at the nanosecond timescale (**Figure S12a**) meaning this molecule could have enough flexibility to bend over itself. The distribution of these distances presents a shoulder at short distance between 5 and 10 Å (**Figure 4c**), mainly due to π-π stacking between two aromatic rings of the same molecule. The intra-molecular and extra-molecular π-π stacking are the main interactions arising between BDF molecules in the blends. From PLA-BDF20 to PLA-

BDF30, there is a significant increase of π-π stacking interactions (**Figure 4b,d,e**). This supports the importance of the aromatic rings of the BDF evidenced by chemical design study (SAR). The π-π stacking was identified as the main factor for the elastomeric behavior of the blends.

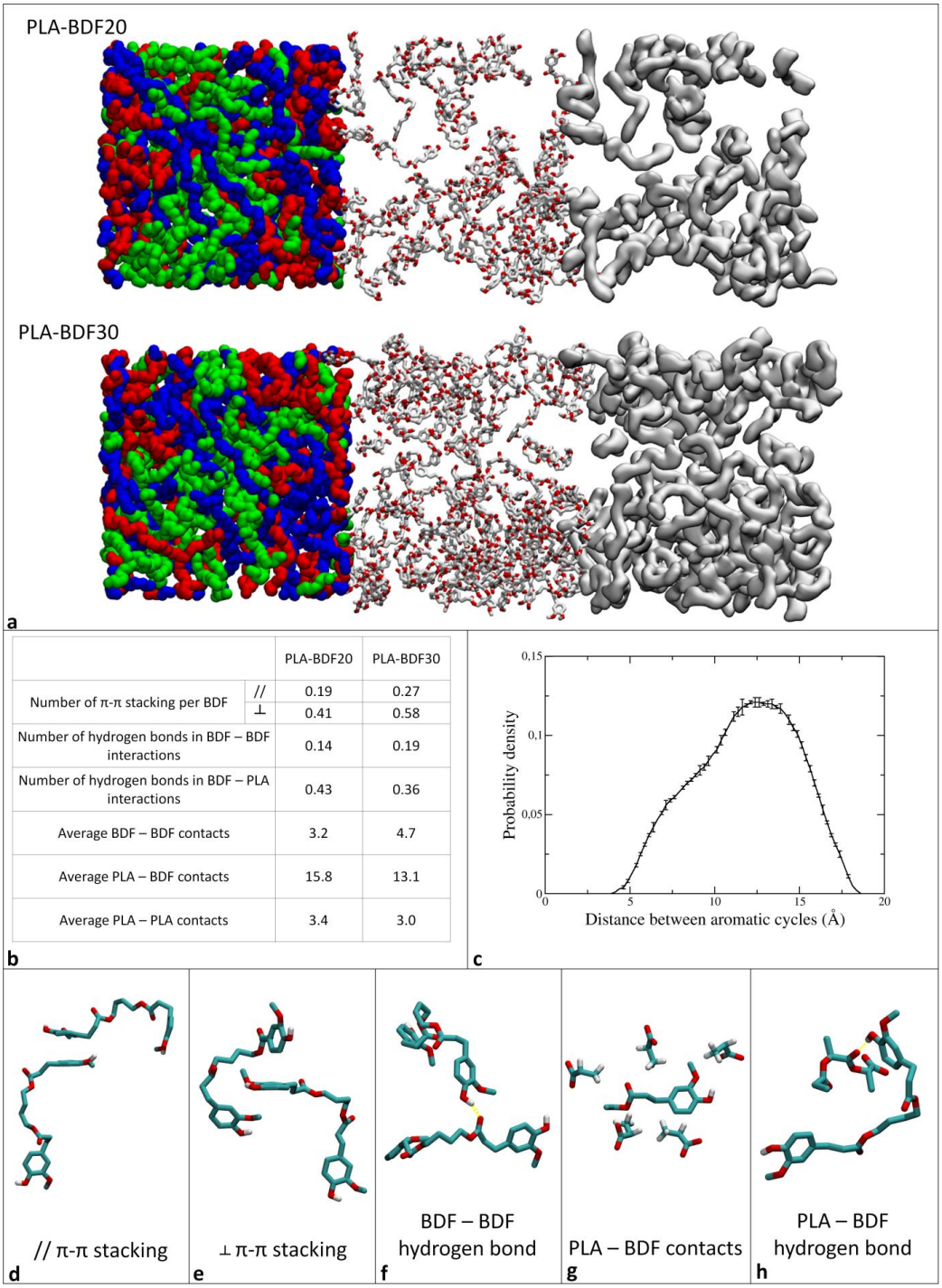

		PLA-BDF20	PLA-BDF30
Number of π-π stacking per BDF	//	0.19	0.27
	⊥	0.41	0.58
Number of hydrogen bonds in BDF – BDF interactions		0.14	0.19
Number of hydrogen bonds in BDF – PLA interactions		0.43	0.36
Average BDF – BDF contacts		3.2	4.7
Average PLA – BDF contacts		15.8	13.1
Average PLA – PLA contacts		3.4	3.0

Figure 4: Simulated systems and quantification of the interactions in PLA-BDF blends.

a. Simulated system of BDF molecules inside PLA chains corresponding to blends of PLA containing 20 wt% and 30 wt% of BDF. The backbone of the three PLA chains is colored in blue, red and green, respectively. BDF molecules (in white with their oxygen atoms in red) are much more isolated in PLA-BDF20 while BDF clusters appear larger in PLA-BDF30. On the right, the surface of the BDF molecules and of their clusters is drawn in white.

b. Quantification of the molecular interactions in blends reveals an increase of the π-π stacking interactions by 50% in PLA-BDF30 compared to PLA-BDF20; this is in concordance with a significant increase of the average BDF-BDF contacts. This is consistent with the formation of clusters made of BDF in PLA-BDF30 were the cohesion is mainly driven by π-π stacking.

c. Distribution of the distance between the center of mass of the two BDF aromatic cycles in PLA-BDF30. It indicates the BDF molecules have the ability to bend and to extend regarding their chemical environment. The asymmetrical distributions show a higher probability density between 5 and 10 Å corresponding to an increase of bended BDF in correlation with the increase of π-π stacking interactions.

d. Parallel π-π stacking interaction between two molecules of BDF extracted from the simulation.

e. Perpendicular π-π stacking interaction between two molecules of BDF extracted from the simulation.

f. Hydrogen bond formed between two molecules of BDF extracted from the simulation.

g. Contacts between a half part of a molecule of BDF (approximately corresponding to a ferulic acid moiety) and five polylactic acid monomers (coming from more than one PLA chain) extracted from the simulation.

h. Hydrogen bond formed between a polylactic acid monomers and a molecule of BDF extracted from the simulation.

The formation of large clusters in PLA-BDF30 is in full accordance with the DSC and XRD characterizations. Such clusters, where a sufficient amount of BDF molecules has no contact at all with PLA, are able to crystallize. On the contrary, loose clusters of BDF in PLA-BDF20 would not crystallize as every single molecule of BDF always has contacts with PLA. Modelling results are consistent with thermal and structural characterization depicting a phase separation starting at a critical content of BDF. This phase separation coincides with the transition from plastic to elastomeric behavior reported by tensile experiments (**Figure 1a**).

Until a content of 20 wt%, BDF is fully miscible in PLA due to a favorable functional spacing of hydrophobic and hydrophilic moieties ensuring numerous contacts and van der Waals interactions and acts as a plasticizer easing the plastic deformation (**Figure 5b**). At 30 wt% BDF, a significant phase separation occurs leading to the formation of large clusters of BDF in PLA and an elastomeric behavior of the blend is reported (**Figure 5c**). With this hypothesis, the cohesion of the blend is maintained despite the phase separation thanks to the high affinities between PLA and BDF at the interface ("PLA–BDF" interactions) and to the π-π stacking interactions in the clusters of BDF molecules ("BDF–BDF" interactions). The elastomeric behavior would result from the π-π stacking between BDF molecules creating netpoints as previously reported in literature for others materials with shape memory effect (Figure 5c).[48,49]

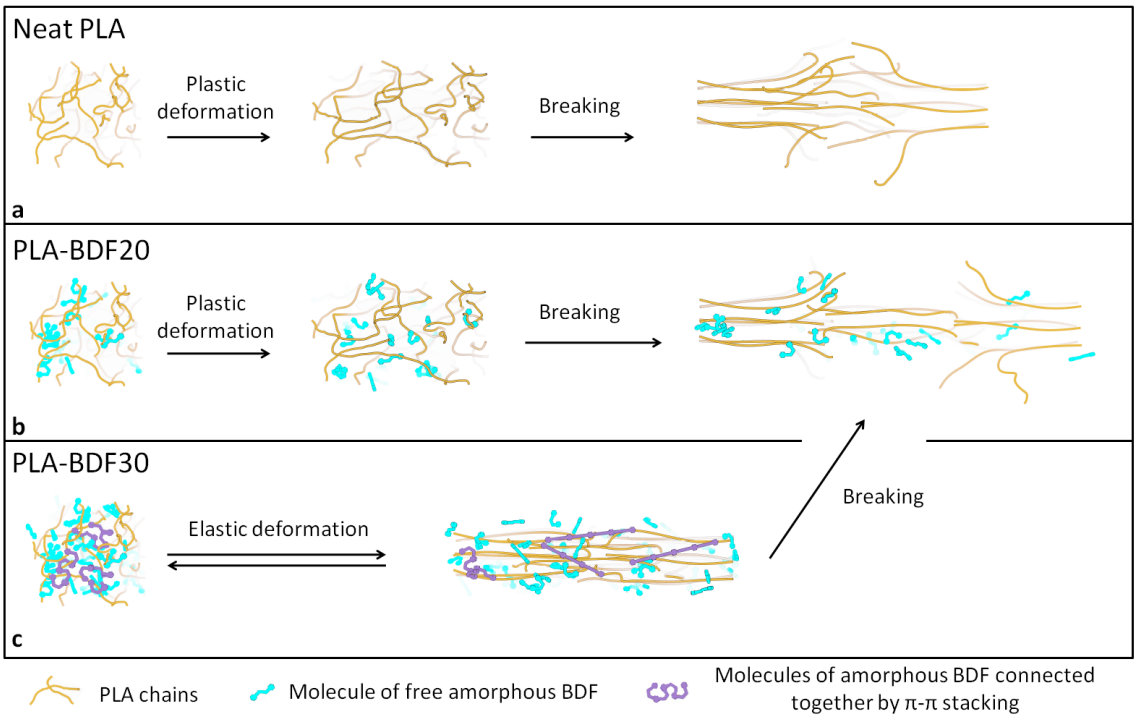

Figure 5: Mechanism of thermoplastic to elastomeric transition behavior in PLA-BDF blends.

a. Molecules of PLA before and after plastic deformation. When the deformation is too high for the weak interactions to handle, the chains are separated and the material breaks.

b. Molecules of PLA blended with 20 wt% BDF. The BDF molecules have good chemical affinities with PLA. At this content, the molecules of BDF act as plasticizer easing the plastic deformation.

c. Molecules of PLA blended with 30 wt% of BDF. At this content, the BDF molecules creates small clusters. The cohesion in the material is maintained by PLA-BDF interactions combined with BDF-BDF interactions, which are mainly driven by π-π stacking bonding.

4. Conclusion

Hot-melting a critical amount of ferulic acid derivative (BDF) with PLA yields an elastomeric blend with shape-memory behavior. Blending BDF preserved the transparency of PLA in the visible wavelengths while providing absorbance in most UV spectrum. The absence of chemical reagent (e.g., crosslinker, curing agent, catalyst) and the ease of processability make this blend easy to prepare and to scale-up. This material is a safe and sustainable alternative to oil-based and non-compostable/recyclable elastomers and thermoplastic elastomers. Further, BDF does not exhibit any endocrine disruption activity while the compostability and recyclability of the PLA-BDF blends should not be hindered as (1) there is no covalent crosslinking, and (2) BDF is chemically recyclable and allegedly compostable due to its hydrolysable ester moieties. Structure-activity relationship analysis combined to molecular modelling supports the proposed structural mechanism where the elastomeric blends contain clusters of BDF molecules inter-connected by π-π stacking in a PLA network. The formation of these clusters in PLA occurs above a BDF threshold content of 25 wt% corresponding to phase separation. Three key parameters are required for the additive to maintain cohesion in the blends: (1) inter- and intra-molecular π-π stacking, (2) hydrophobic and hydrophilic functionalities positioned suitably with the architecture of the polymer, and (3) molecular flexibility. We speculate this elastomeric behavior can be reproduced in different bio-based polymers with analog additives leading to novel families of bio-elastomers suitable for recycling and biological degradation leading to a class of fully sustainable thermoplastic elastomers.

ASSOCIATED CONTENT

Preparation of materials (Figures S1 to S2, Table S1), UV-Vis spectroscopy (Figure S3), Thermal characterizations (Figure S4, Table S2), Chemical characterizations (Table S3), XRD characterizations (Figures S5 to S6), Modelling data (Table S4, Figures S7 to S9), Shape

Memory Cycle and Shape Memory qualitative analyses (Figure S10, Movies S1 and S2, Caption for movies S2). This material is available free of charge via the Internet at http://pubs.acs.org.

AUTHOR INFORMATION

Corresponding Authors

florent.allais@agroparistech.fr

antoine.gallos@agroparistech.fr

ORCID numbers

0000-0001-8711-1421 Antoine Gallos

0000-0002-9252-2396 Jean-Marc Crowet

0000-0001-8785-6191 Laurent Michely

0000-0001-9524-1314 Vikram Raghuwanshi

0000-0002-2309-9870 Matthieu Mention

0000-0003-4031-6838 Valérie Langlois

0000-0002-6743-7915 Manuel Dauchez

0000-0003-3512-0056 Gil Garnier

0000-0003-4132-6210 Florent Allais

Author Contributions

A.G., F.A. and G.G. led and designed the study. J.M.C. and M.D. performed the modeling analyses. M.M. performed the synthesis of the additives. A.G. performed the melt blending and the injection of the materials. A.G. performed DSC and GPC analyses. V.R. performed the tensile testing. L.M. and V.L. performed the DMA and the DRX analyses. A.G. prepared the first draft of the manuscript with the data coming from all of the authors. J.M. wrote the modeling part. A.G., J.M., G.G., F.A., V.L. and M.D. revised the manuscript.

Note

This work was patented.

FUNDING

This research was funded by the *Région Grand Est*, the *Conseil Départemental de la Marne,* the *Grand Reims and the chair of research MAgICS*.

ACKNOWLEDGMENT

The *Région Grand Est*, the *Conseil Départemental de la Marne* and the *Grand Reims* are gratefully acknowledged for supporting these works. The authors thank both ROMEO and Multiscale Molecular Modelling platforms for providing CPU hours, and the chair of research MAgICS for fundings. Hua Wong is gratefully acknowledged for the design of the figure 5. The *Institut National de Recherche pour l'Agriculture, l'Alimentation et l'Environnement (INRAE)* and the *Unité Mixte de Recherche Fractionnement des AgroRessources et Environnement (UMR FARE)* are acknowledged for letting us access to their equipment. Alain Lemaitre (UMR FARE) is acknowledged for his kind help with the injection process.

REFERENCES

(1) Miller, S. A. Sustainable Polymers: Opportunities for the next Decade. *ACS Macro Lett.* **2013**, *2* (6), 550–554. https://doi.org/10.1021/mz400207g.

(2) Gross, R. A.; Kalra, B. Biodegradable Polymers for the Environment. *Science (80-.).* **2002**, *297* (5582), 803–807. https://doi.org/10.1126/science.297.5582.803.

(3) Soroudi, A.; Jakubowicz, I. Recycling of Bioplastics, Their Blends and Biocomposites: A Review. *Eur. Polym. J.* **2013**, *49* (10), 2839–2858. https://doi.org/10.1016/j.eurpolymj.2013.07.025.

(4) Auras, R.; Harte, B.; Selke, S. An Overview of Polylactides as Packaging Materials. *Macromol. Biosci.* **2004**, *4* (9), 835–864. https://doi.org/10.1002/mabi.200400043.

(5) Lasprilla, A. J. R.; Martinez, G. A. R.; Lunelli, B. H.; Jardini, A. L.; Filho, R. M. Poly-Lactic Acid Synthesis for Application in Biomedical Devices - A Review. *Biotechnol. Adv.* **2012**, *30* (1), 321–328. https://doi.org/10.1016/j.biotechadv.2011.06.019.

(6) Gallos, A.; Fontaine, G.; Bourbigot, S. Reactive Extrusion of Stereocomplexed Poly-L, d -Lactides: Processing, Characterization, and Properties. *Macromol. Mater. Eng.* **2013**, *298* (9), 1016–1023. https://doi.org/10.1002/mame.201200271.

(7) Tsuji, H. Poly(Lactic Acid) Stereocomplexes: A Decade of Progress. *Adv. Drug Delivery Rev.* **2016**, *107*, 97–135. https://doi.org/10.1016/j.addr.2016.04.017.

(8) Raquez, J. M.; Habibi, Y.; Murariu, M.; Dubois, P. Polylactide (PLA)-Based Nanocomposites. *Prog. Polym. Sci.* **2013**, *38* (10–11), 1504–1542. https://doi.org/10.1016/j.progpolymsci.2013.05.014.

(9) Rahman, M.; Brazel, C. S. The Plasticizer Market: An Assessment of Traditional Plasticizers and Research Trends to Meet New Challenges. *Prog. Polym. Sci.* **2004**, *29* (12), 1223–1248. https://doi.org/10.1016/j.progpolymsci.2004.10.001.

(10) Mekonnen, T.; Mussone, P.; Khalil, H.; Bressler, D. Progress in Bio-Based Plastics and Plasticizing Modifications. *J. Mater. Chem. A* **2013**, *1* (43), 13379–13398. https://doi.org/10.1039/C3TA12555F.

(11) Murariu, M.; Dubois, P. PLA Composites: From Production to Properties. *Adv. Drug Deliv. Rev.* **2016**, *107*, 17–46. https://doi.org/10.1016/j.addr.2016.04.003.

(12) Martin, O.; Avérous, L. Poly(Lactic Acid): Plasticization and Properties of Biodegradable Multiphase Systems. *Polymer (Guildf).* **2001**, *42* (14), 6209–6219. https://doi.org/10.1016/S0032-3861(01)00086-6.

(13) Kfoury, G.; Raquez, J.-M.; Hassouna, F.; Odent, J.; Toniazzo, V.; Ruch, D.; Dubois, P. Recent Advances in High Performance Poly(Lactide): From "Green" Plasticization to Super-Tough Materials via (Reactive) Compounding. *Front. Chem.* **2013**, *1*, 32. https://doi.org/10.3389/fchem.2013.00032.

(14) Lai, S.-M.; Lan, Y.-C. Shape Memory Properties of Melt-Blended Polylactic Acid (PLA)/Thermoplastic Polyurethane (TPU) Bio-Based Blends. *J. Polym. Res.* **2013**, *20* (5), 140. https://doi.org/10.1007/s10965-013-0140-6.

(15) Zhang, W.; Chen, L.; Zhang, Y. Surprising Shape-Memory Effect of Polylactide Resulted from Toughening by Polyamide Elastomer. *Polymer (Guildf).* **2009**, *50* (5), 1311–1315. https://doi.org/10.1016/j.polymer.2009.01.032.

(16) Tsuji, H.; Ikada, Y. Blends of Aliphatic Polyesters. I. Physical Properties and Morphologies of Solution-Cast Blends from Poly(DL-Lactide) and Poly(Ɛ-Caprolactone). *J. Appl. Polym. Sci.* **1996**, *60* (13), 2367–2375. https://doi.org/10.1002/(SICI)1097-4628(19960627)60:13<2367::AID-APP8>3.0.CO;2-C.

(17) Simón, D.; Borreguero, A. M.; de Lucas, A.; Rodríguez, J. F. Recycling of Polyurethanes

from Laboratory to Industry, a Journey towards the Sustainability. *Waste Manage.* **2018**, *76*, 147–171. https://doi.org/10.1016/j.wasman.2018.03.041.

(18) Fazli, A.; Rodrigue, D. Waste Rubber Recycling: A Review on the Evolution and Properties of Thermoplastic Elastomers. *Materials* **2020**, *13* (3), 782. https://doi.org/10.3390/ma13030782.

(19) Coran, A. Y. Chemistry of the Vulcanization and Protection of Elastomers: A Review of the Achievements. *J. Appl. Polym. Sci.* **2003**, *87* (1), 24–30. https://doi.org/10.1002/app.11659.

(20) Asaro, L.; Gratton, M.; Seghar, S.; Aït Hocine, N. Recycling of Rubber Wastes by Devulcanization. *Resour., Conserv. Recycl.* **2018**, *133*, 250–262. https://doi.org/10.1016/j.resconrec.2018.02.016.

(21) Pion, F.; Reano, A. F.; Ducrot, P.-H.; Allais, F. Chemo-Enzymatic Preparation of New Bio-Based Bis-and Trisphenols: New Versatile Building Blocks for Polymer Chemistry. *RSC Adv.* **2013**, *3* (23), 8988–8997. https://doi.org/10.1039/c3ra41247d.

(22) Teixeira, A. R. S.; Willig, G.; Couvreur, J.; Flourat, A. L.; Peru, A. A. M.; Ferchaud, P.; Ducatel, H.; Allais, F. From Bench Scale to Kilolab Production of Renewable Ferulic Acid-Based Bisphenols: Optimisation and Evaluation of Different Purification Approaches towards Technical Feasibility and Process Environmental Sustainability. *React. Chem. Eng.* **2017**, *2* (3), 406–419. https://doi.org/10.1039/c7re00017k.

(23) Maiorana, A.; Reano, A. F.; Centore, R.; Grimaldi, M.; Balaguer, P.; Allais, F.; Gross, R. A. Structure Property Relationships of Biobased: N -Alkyl Bisferulate Epoxy Resins. *Green Chem.* **2016**, *18* (18), 4961–4973. https://doi.org/10.1039/c6gc01308b.

(24) Wang, Y.; Su, J.; Li, T.; Ma, P.; Bai, H.; Xie, Y.; Chen, M.; Dong, W. A Novel UV-

Shielding and Transparent Polymer Film: When Bioinspired Dopamine–Melanin Hollow Nanoparticles Join Polymers. *ACS Appl. Mater. Interfaces* **2017**, *9* (41), 36281–36289. https://doi.org/10.1021/acsami.7b08763.

(25) Backes, E. H.; Pires, L. de N.; Costa, L. C.; Passador, F. R.; Pessan, L. A. Analysis of the Degradation During Melt Processing of PLA/Biosilicate® Composites. *J. Compos. Sci.* **2019**, *3* (2), 52. https://doi.org/10.3390/jcs3020052.

(26) Oulame, M. Z.; Pion, F.; Allauddin, S.; Raju, K. V. S. N.; Ducrot, P.-H.; Allais, F. Renewable Alternating Aliphatic-Aromatic Poly(Ester-Urethane)s Prepared from Ferulic Acid and Bio-Based Diols. *Eur. Polym. J.* **2015**, *63*, 186–193. https://doi.org/10.1016/j.eurpolymj.2014.11.031.

(27) Sawpan, M. A.; Pickering, K. L.; Fernyhough, A. Improvement of Mechanical Performance of Industrial Hemp Fibre Reinforced Polylactide Biocomposites. *Composites, Part A* **2011**, *42* (3), 310–319. https://doi.org/10.1016/j.compositesa.2010.12.004.

(28) Pluta, M.; Galeski, A.; Alexandre, M.; Paul, M. A.; Dubois, P. Polylactide/Montmorillonite Nanocomposites and Microcomposites Prepared by Melt Blending: Structure and Some Physical Properties. *J. Appl. Polym. Sci.* **2002**, *86* (6), 1497–1506. https://doi.org/10.1002/app.11309.

(29) Kawai, T.; Rahman, N.; Matsuba, G.; Nishida, K.; Kanaya, T.; Nakano, M.; Okamoto, H.; Kawada, J.; Usuki, A.; Honma, N.; Nakajima, K.; Matsuda, M. Crystallization and Melting Behavior of Poly (L-Lactic Acid). *Macromolecules* **2007**, *40* (26), 9463–9469. https://doi.org/10.1021/ma070082c.

(30) Chen, X.; Kalish, J.; Hsu, S. L. Structure Evolution of A′-Phase Poly(Lactic Acid). *J.*

Polym. Sci., Part B: Polym. Phys. **2011**, *49* (20), 1446–1454. https://doi.org/10.1002/polb.22327.

(31) Wasanasuk, K.; Tashiro, K. Crystal Structure and Disorder in Poly(l-Lactic Acid) δ Form (A′ Form) and the Phase Transition Mechanism to the Ordered α Form. *Polymer (Guildf).* **2011**, *52* (26), 6097–6109. https://doi.org/10.1016/j.polymer.2011.10.046.

(32) Wang, J.; Wolf, R. M.; Caldwell, J. W.; Kollman, P. A.; Case, D. A. Development and Testing of a General Amber Force Field. *J. Comput. Chem.* **2004**, *25* (9), 1157–1174. https://doi.org/10.1002/jcc.20035.

(33) Zheng, X. Q.; Li, L. Te; Liu, X. L.; Wang, X. J.; Lin, J.; Li, D. Production of Hydrolysate with Antioxidative Activity by Enzymatic Hydrolysis of Extruded Corn Gluten. *Appl. Microbiol. Biotechnol.* **2006**, *73* (4), 763–770. https://doi.org/10.1007/s00253-006-0537-9.

(34) Glova, A. D.; Falkovich, S. G.; Dmitrienko, D. I.; Lyulin, A. V.; Larin, S. V.; Nazarychev, V. M.; Karttunen, M.; Lyulin, S. V. Scale-Dependent Miscibility of Polylactide and Polyhydroxybutyrate: Molecular Dynamics Simulations. *Macromolecules* **2018**, *51* (2), 552–563. https://doi.org/10.1021/acs.macromol.7b01640.

(35) McAliley, J. H.; Bruce, D. A. Development of Force Field Parameters for Molecular Simulation of Polylactide. *J. Chem. Theory Comput.* **2011**, *7* (11), 3756–3767. https://doi.org/10.1021/ct200251x.

(36) Berendsen, H. J. C.; Postma, J. P. M.; van Gunsteren, W. F.; DiNola, A.; Haak, J. R. Molecular Dynamics with Coupling to an External Bath. *J. Chem. Phys.* **1984**, *81* (8), 3684–3690. https://doi.org/10.1063/1.448118.

(37) Essmann, U.; Perera, L.; Berkowitz, M. L.; Darden, T.; Lee, H.; Pedersen, L. G. A Smooth Particle Mesh Ewald Method. *J. Chem. Phys.* **1995**, *103* (19), 8577–8593.

https://doi.org/10.1063/1.470117.

(38) Abraham, M. J.; Murtola, T.; Schulz, R.; Páll, S.; Smith, J. C.; Hess, B.; Lindahl, E. GROMACS: High Performance Molecular Simulations through Multi-Level Parallelism from Laptops to Supercomputers. *Softwarex* **2015**, *1–2*, 19–25. https://doi.org/10.1016/J.SOFTX.2015.06.001.

(39) Michaud-Agrawal, N.; Denning, E. J.; Woolf, T. B.; Beckstein, O. MDAnalysis: A Toolkit for the Analysis of Molecular Dynamics Simulations. *J. Comput. Chem.* **2011**, *32* (10), 2319–2327. https://doi.org/10.1002/jcc.21787.

(40) Humphrey, W.; Dalke, A.; Schulten, K. VMD: Visual Molecular Dynamics. *J. Mol. Graphics* **1996**, *14* (1), 33–38. https://doi.org/10.1016/0263-7855(96)00018-5.

(41) Fu, C.-F.; Tian, S. X. A Comparative Study for Molecular Dynamics Simulations of Liquid Benzene. *J. Chem. Theory Comput.* **2011**, *7* (7), 2240–2252. https://doi.org/10.1021/ct2002122.

(42) Shtarkman, B. P.; Razinskaya, I. N. Plasticization Mechanism and Structure of Polymers. *Acta Polym.* **1983**, *34* (8), 514–520. https://doi.org/10.1002/actp.1983.010340812.

(43) Casalini, R.; Ngai, K. L.; Robertson, C. G.; Roland, C. M. A α- and β-Relaxations in Neat and Antiplasticized Polybutadiene. *J. Polym. Sci., Part B: Polym. Phys.* **2000**, *38* (14), 1841–1847. https://doi.org/10.1002/1099-0488(20000715)38:14<1841::AID-POLB20>3.0.CO;2-0.

(44) Pillin, I.; Montrelay, N.; Grohens, Y. Thermo-Mechanical Characterization of Plasticized PLA: Is the Miscibility the Only Significant Factor? *Polymer (Guildf).* **2006**, *47* (13), 4676–4682. https://doi.org/10.1016/J.POLYMER.2006.04.013.

(45) Ljungberg, N.; Wesslén, B. Tributyl Citrate Oligomers as Plasticizers for Poly (Lactic

Acid): Thermo-Mechanical Film Properties and Aging. *Polymer (Guildf).* **2003**, *44* (25), 7679–7688. https://doi.org/10.1016/j.polymer.2003.09.055.

(46) Mention, M. M.; Flourat, A. L.; Peyrot, C.; Allais, F. Biomimetic Regioselective and High-Yielding Cu(I)-Catalyzed Dimerization of Sinapate Esters in Green Solvent Cyrene^{TM}: Towards Sustainable Antioxidant and Anti-UV Ingredients. *Green Chem.* **2020**, *22* (6), 2077–2085. https://doi.org/10.1039/D0GC00122H.

(47) Pilate, F.; Toncheva, A.; Dubois, P.; Raquez, J. M. Shape-Memory Polymers for Multiple Applications in the Materials World. *Eur. Polym. J.* **2016**, *80*, 268–294. https://doi.org/10.1016/j.eurpolymj.2016.05.004.

(48) Yang, R.; Chen, L.; Ruan, C.; Zhong, H.-Y.; Wang, Y.-Z. Chain Folding in Main-Chain Liquid Crystalline Polyesters: From π–π Stacking toward Shape Memory. *J. Mater. Chem. C* **2014**, *2* (30), 6155. https://doi.org/10.1039/C4TC00512K.

(49) Li, M.; Song, F.; Chen, L.; Wang, X.; Wang, Y. Flexible Material Based on Poly(Lactic Acid) and Liquid Crystal with Multishape Memory Effects. *ACS Sustainable Chem. Eng.* **2016**, *4* (7), 3820–3829. https://doi.org/10.1021/acssuschemeng.6b00582.

Blending a critical amount of a bio-based ferulic acid derivative turns a thermoplastic polylactic acid into an elastomeric blend with shape-memory behavior. The transparency of the polylactic acid is preserved while the absorbance in UV wavelength is improved. The cohesion in such elastomeric blend appears to be maintained by non-covalent interaction only.